Vibration Analysis of Thin/Thick, Composites/Metallic Spinning Cylindrical Shells by Refined Beam Models

E. Carrera
Professor of Aerospace Structures and Aeroelasticity,
Department of Mechanical and Aerospace Engineering,
Politecnico di Torino,
Corso Duca degli Abruzzi 24,
Torino 10129, Italy;
School of Aerospace, Mechanical and Manufacturing Engineering,
RMIT University,
124 La Trobe Street,
Melbourne 3000, Australia
e-mail: erasmo.carrera@polito.it

M. Filippi
Department of Mechanical and Aerospace Engineering,
Politecnico di Torino,
Corso Duca degli Abruzzi 24,
Torino 10129, Italy,
e-mail: matteo.filippi@polito.it

This paper evaluates the vibration characteristics of thin/thick rotating cylindrical shells made of metallic and composite materials. A previous theory of the authors is extended here to include the effects of geometrical stiffness due to rotation. To this end, variable kinematic one-dimensional (1D) models obtained by applying the Carrera Unified Formulation (CUF) were used. The components of the displacement fields are x, z polynomials of arbitrary order N, making it possible to go beyond the rigid cross section assumptions of the classical beam theories. A significant contribution of this formulation consists in the possibility to include the in-plane cross-sectional deformations allowing the introduction of the in-plane initial stress effects, e.g., the effect of the geometrical stiffness. Equations of motions, including both Coriolis and in-plane initial stress contributions, were solved through the finite element method. Several analyses were carried out on both thin and thick cylinders made of either metallic or composite materials with different boundary conditions. The results are compared with analytical and numerical shell formulations and three-dimensional solutions available in the literature. Various laminate lay-up have been considered in the case of composites shells. Numerical evaluations of the effect of geometric stiffness are provided, demonstrating its importance in the analyses presented. The 1D models appear very effective to investigate the dynamics of spinning shells and, contrary to shell theories, they do not require any amendments with thick shell geometry. From the computational point of view, the present refined beam models are less expensive than the shell and solid counterparts. [DOI: 10.1115/1.4029688]

1 Introduction

Many engineering applications require the use of rotating structures, whose design can represent a crucial element of the whole project. Thus, a number of theories have been developed in order to describe the dynamics of the different spinning structures.

Beam theories have been extensively used to investigate the critical speeds and instabilities of shafts made of either isotropic [1–3] or composite [4,5] materials. Although interesting attempts to improve the classical theories have been proposed [6,7], the 1D theories have been limited to the study of rotors whose cross sections remain largely undeformed. However, when thin disks or thin-walled structures are considered, this assumption becomes unacceptable and, therefore, more complex mathematical models are required. The analysis of rotating cylinders has given a great impulse to the use of shell theories in the rotordynamics, which is confirmed by the vast number of papers available in the literature. The earliest results were presented by Bryan in 1890 [8], who extended a spinning ring theory to describe the behavior of rotating shells. Later, Srinivasan and Lauterbach [9] investigated the Coriolis and centrifugal effects on the forward and backward-traveling waves of long and thin cylindrical shells. In Ref. [10], Padovan considered the same structures subjected to axial, radial, and torsional prestress. The generality of his solution makes it possible to handle the material anisotropy as well as arbitrary boundary conditions. These results together with experimental tests were used as references in order to assess the ring theory proposed in Ref. [11]. Then, in Ref. [12], this theory led to interesting results for the finite length rotating shells also with both ends clamped. Further theories were presented in Refs. [13–16], in which the finite element and differential quadrature methods (DQMs) were used considering both thin and thick cylinders. Recently in Ref. [17], Sun et al. used the Fourier series expansion method and Sander shell theory to develop an analytical solution valid for any type of classical boundary conditions. Interesting parametric analyses were carried out on thin shells. Moreover, with the wide spread of the composite materials in the design of rotors, the analysis of the spinning cylinders has required further improvements of the theoretical models. Lam and Loy compared the accuracy in the computation of forward and backward frequencies of simply supported laminate cylinders of four different thin shell theories obtained through a unified approach [18,19]. Concluding that Love theory assures good accuracy for large values of the length-to-radius ratio, in Ref. [20], the authors investigated the effects of boundary conditions for thin spinning cylindrical shells. In addition, using the same displacement formulation, Civalek studied the dynamic behaviors of orthotropic cylinders with the method of discrete singular convolution [21]. In contrast to the equivalent single layer approach of the above papers, in Ref. [22], Ramezani and Ahmadian conceived a layer-wise theory combined with a wave propagation approach. Shell theories have been also used to analyze the rotating stiffened cylinders. For instance, in Ref. [23], the equations of motion of ring-stiffened shells were solved by using the Rayleigh–Ritz method and the Sander shell theory. The arbitrary boundary conditions were imposed by means of artificial stiffness at the end of the structure. The effects of the number as well as the dimensions of the rings have been investigated. As far as spinning composite structures are concerned, in Refs. [24] and [25], two energy approaches were employed to determine the influences of stringers and rings on the dynamic characteristics. In Ref. [25], the stiffness contributions due to the stiffeners were treated as both discrete and distributed quantities. The averaging method yielded to inaccurate results when the number of stiffeners is small. As

Contributed by the Technical Committee on Vibration and Sound of ASME for publication in the JOURNAL OF VIBRATION AND ACOUSTICS. Manuscript received March 31, 2014; final manuscript received January 28, 2015; published online March 13, 2015. Assoc. Editor: Yukio Ishida.

stated before, the number of two-dimensional theories for the study of rotating shells is impressive and, a comprehensive overview can be found in Ref. [26].

The present paper aims to introduce and compare a variety of refined 1D beam models in order to study the dynamics of rotating cylindrical shells. These theories are obtained through the CUF [27], which makes it possible, at least theoretically, to derive an infinite number of refined displacements models. Various papers have proved that, with a lower number of degrees of freedom, the higher-order 1D theories furnish results very close to those by the two- or three-dimensional solutions also when the structures are thin-walled [28] or constituted by composite materials [29,30]. Recently in Refs. [31] and [32], CUF has been extended to the study of the critical speeds and stability of isotropic and composite shafts providing encouraging results. So far, only the Coriolis effect has been included in the formulation, since the structures have considered rigid cross sections. Nevertheless, when the cross sections undergo large deformations the hoop tension is essential to avoid inaccurate predictions of the frequency evolutions and, for this reason, this term is taken into account here in order to handle the rotating shells. One of the main contribution of this work is that, besides the thin cylinders, the present beam formulation makes it possible to consider the thick shells, which usually require further improvements of the classical two-dimensional approaches [15].

In order to assess the new theory, several linear analyses have been carried out on isotropic and laminated thin/thick cylinders, and the related results have been compared with the solutions presented in the literature.

2 One-Dimensional Theories Through the Unified Formulation

The 1D-CUF states that the displacement field in Cartesian coordinates, $\mathbf{u}(x, y, z, t)$, is an expansion of arbitrary functions of the cross section coordinates $F_\tau(x, z)$, for the displacement vector, $\mathbf{u}_\tau(y)$

$$\mathbf{u}(x,y,z,t) = F_\tau(x,z)\mathbf{u}_\tau(y,t) \qquad \tau = 1,2,\ldots,T \tag{1}$$

where T is the number of terms in the expansion and, in according to the generalized Einstein's notation, τ indicates summation. In this work, Eq. (1) consists of Taylor-like expansions, hereinafter referred to as "TE." For example, the second-order displacement field "TE2" is

$$\begin{aligned} u_x &= u_{x_1} + x\,u_{x_2} + z\,u_{x_3} + x^2\,u_{x_4} + xz\,u_{x_5} + z^2\,u_{x_6} \\ u_y &= u_{y_1} + x\,u_{y_2} + z\,u_{y_3} + x^2\,u_{y_4} + xz\,u_{y_5} + z^2\,u_{y_6} \\ u_z &= u_{z_1} + x\,u_{z_2} + z\,u_{z_3} + x^2\,u_{z_4} + xz\,u_{z_5} + z^2\,u_{z_6} \end{aligned} \tag{2}$$

while the third-order displacement field "TE3" becomes

$$\begin{aligned} u_x &= u_{x_1} + x\,u_{x_2} + z\,u_{x_3} + x^2\,u_{x_4} + xz\,u_{x_5} + z^2\,u_{x_6} \\ &\quad + x^3\,u_{x_7} + x^2z\,u_{x_8} + xz^2\,u_{x_9} + z^3\,u_{x_{10}} \\ u_y &= u_{y_1} + x\,u_{y_2} + z\,u_{y_3} + x^2\,u_{y_4} + xz\,u_{y_5} + z^2\,u_{y_6} \\ &\quad + x^3\,u_{y_7} + x^2z\,u_{y_8} + xz^2\,u_{y_9} + z^3\,u_{y_{10}} \\ u_z &= u_{z_1} + x\,u_{z_2} + z\,u_{z_3} + x^2\,u_{z_4} + xz\,u_{z_5} + z^2\,u_{z_6} \\ &\quad + x^3\,u_{z_7} + x^2z\,u_{z_8} + xz^2\,u_{z_9} + z^3\,u_{z_{10}} \end{aligned} \tag{3}$$

A remarkable feature is that classical beam theories are obtainable as particular cases of Taylor-like expansions. It should be noted that classical theories require reduced material stiffness coefficients to contrast Poisson's locking. Unless otherwise specified, for classical and first-order models, Poisson's locking is corrected according to Carrera et al. [27]. The stresses and the strains are grouped as it follows:

$$\begin{aligned} \boldsymbol{\epsilon}_p &= \{\epsilon_{zz} \quad \epsilon_{xx} \quad \epsilon_{xz}\}^{\mathrm{T}} & \boldsymbol{\sigma}_p &= \{\sigma_{zz} \quad \sigma_{xx} \quad \sigma_{xz}\}^{\mathrm{T}} \\ \boldsymbol{\epsilon}_n &= \{\epsilon_{zy} \quad \epsilon_{xy} \quad \epsilon_{yy}\}^{\mathrm{T}} & \boldsymbol{\sigma}_n &= \{\sigma_{zy} \quad \sigma_{xy} \quad \sigma_{yy}\}^{\mathrm{T}} \end{aligned} \tag{4}$$

The subscript "p" stands for terms lying on the cross section, while "n" stands for terms lying on the other planes, which are orthogonal to the cross section. The linear strain–displacement relations and Hooke's law are, respectively,

$$\begin{aligned} \boldsymbol{\epsilon}_p &= \mathbf{D}_p\mathbf{u} \\ \boldsymbol{\epsilon}_n &= (\mathbf{D}_{ny} + \mathbf{D}_{np})\mathbf{u} \end{aligned} \tag{5}$$

$$\begin{aligned} \boldsymbol{\sigma}_p &= \tilde{\mathbf{C}}_{pp}\boldsymbol{\epsilon}_p + \tilde{\mathbf{C}}_{pn}\boldsymbol{\epsilon}_n \\ \boldsymbol{\sigma}_n &= \tilde{\mathbf{C}}_{np}\boldsymbol{\epsilon}_p + \tilde{\mathbf{C}}_{nn}\boldsymbol{\epsilon}_n \end{aligned} \tag{6}$$

where $\mathbf{D}_p, \mathbf{D}_{ny}$, and $\mathbf{D}_{np}$ are the linear differential operators reported in Ref. [27]. Both box beams and cylinders can be considered constituted by a certain number of either straight or curved plates of orthotropic material, whose material coordinate systems (1, 2, 3) generally do not coincide with the physical coordinate system (x, y, z) (see Fig. 1). Therefore, using this approach, the matrices of material coefficients of the generic material k are

$$\tilde{\mathbf{C}}^k_{pp} = \begin{bmatrix} \tilde{C}^k_{11} & \tilde{C}^k_{12} & \tilde{C}^k_{14} \\ \tilde{C}^k_{12} & \tilde{C}^k_{22} & \tilde{C}^k_{24} \\ \tilde{C}^k_{14} & \tilde{C}^k_{24} & \tilde{C}^k_{44} \end{bmatrix}, \qquad \tilde{\mathbf{C}}^k_{pn} = \begin{bmatrix} \tilde{C}^k_{15} & \tilde{C}^k_{16} & \tilde{C}^k_{13} \\ \tilde{C}^k_{25} & \tilde{C}^k_{26} & \tilde{C}^k_{23} \\ \tilde{C}^k_{45} & \tilde{C}^k_{46} & \tilde{C}^k_{43} \end{bmatrix},$$
$$\tilde{\mathbf{C}}^k_{nn} = \begin{bmatrix} \tilde{C}^k_{55} & \tilde{C}^k_{56} & \tilde{C}^k_{35} \\ \tilde{C}^k_{56} & \tilde{C}^k_{66} & \tilde{C}^k_{36} \\ \tilde{C}^k_{35} & \tilde{C}^k_{36} & \tilde{C}^k_{33} \end{bmatrix} \tag{7}$$

Explicit forms of the coefficients of the matrices $\tilde{\mathbf{C}}$ are reported in Ref. [32]. Since a classical Finite Element technique is adopted in order to deal with arbitrary shaped cross sections, the generalized displacement vector is

$$\mathbf{u}_\tau(y,t) = N_i(y)\mathbf{q}_{\tau i}(t) \tag{8}$$

where $N_i(y)$ are the shape functions and $\mathbf{q}_{\tau i}(t)$ is the nodal displacement vector

$$\mathbf{q}_{\tau i}(t) = \left\{ q_{u_{x_{\tau i}}} \quad q_{u_{y_{\tau i}}} \quad q_{u_{z_{\tau i}}} \right\}^{\mathrm{T}} \tag{9}$$

3 Rotordynamics Equations in CUF Form

In order to obtain the motion equations of a structure that is rotating about its longitudinal axis with a constant speed Ω, Hamilton's principle is used

$$\delta \int_{t_0}^{t_1} (T - (U + U_{\sigma_0}))dt = 0 \tag{10}$$

where T and U are the kinetic and the potential energies in the rotating reference frame, which were previously derived in

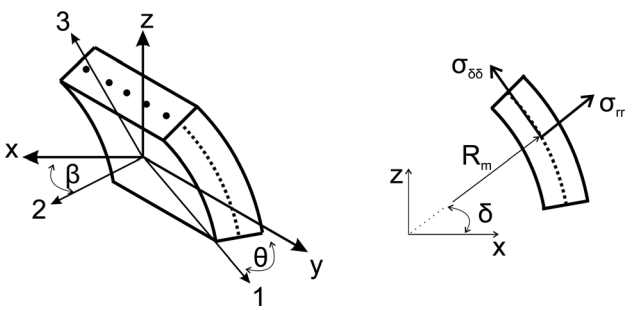

Fig. 1 Physical and material coordinate reference systems

Ref. [31]. The other contribution U_{σ_0} is due to the prestress σ_0 (or prestrain ϵ_0) field, which may be generated by centrifugal or thermal effects. The expression of U_σ is

$$U_{\sigma_0} = \int_V \sigma_0 \epsilon^{\mathrm{nl}} dV \tag{11}$$

where ϵ^{nl} is the nonlinear part of strains. The prestress field for axial-symmetric structures is typically provided in terms of circumferential ($\sigma_{\delta\delta}$), radial (σ_{rr}) and axial (σ_{yy}) contributions that, written in a cartesian coordinate system, are

$$\begin{aligned}
\sigma_{0_{xx}} &= \sigma_{\delta\delta}\sin(\delta)^2 + \sigma_{rr}\cos(\delta)^2 \\
\sigma_{0_{yy}} &= \sigma_{yy} \\
\sigma_{0_{zz}} &= \sigma_{\delta\delta}\cos(\delta)^2 + \sigma_{rr}\sin(\delta)^2 \\
\sigma_{0_{xz}} (= \sigma_{0_{zx}}) &= \sigma_{rr}\sin(\delta)\cos(\delta) - \sigma_{\delta\delta}\sin(\delta)\cos(\delta)
\end{aligned}$$

In this work, unless differently specified, the initial stress acts in the circumferential direction, and it is equal to $\sigma_{\delta\delta} = \rho\Omega^2 R_{\mathrm{m}}^2$, where ρ is the material density and R_{m} is the mean radius. Disregarding the axial prestress, the geometrical potential energy becomes

$$U_{\sigma_0} = \int_V \sigma_{0_{xx}}\epsilon_{xx}^{\mathrm{nl}} + \sigma_{0_{zz}}\epsilon_{zz}^{\mathrm{nl}} + \sigma_{0_{xz}}\epsilon_{xz}^{\mathrm{nl}} + \sigma_{0_{zx}}\epsilon_{zx}^{\mathrm{nl}} dV \tag{12}$$

Using Eqs. (1) and (8), Eq. (10) becomes

$$\begin{aligned}
\int_{t_0}^{t_1} \Big(& \delta\mathbf{q}_{\tau i}^T \mathbf{M}^{ij\tau s}\mathbf{q}_{sj} + \delta\mathbf{q}_{\tau i}^T \mathbf{G}_\Omega^{ij\tau s}\dot{\mathbf{q}}_{sj} \\
& + \delta\mathbf{q}_{\tau i}^T \Big(\mathbf{K}^{ij\tau s} + \mathbf{K}_{\sigma_0}^{ij\tau s} - \mathbf{K}_\Omega^{ij\tau s}\Big)\mathbf{q}_{sj} + \delta\mathbf{q}_{\tau i}^T \mathbf{F}_\Omega^{i\tau}\mathbf{r}\Big) dt = 0
\end{aligned} \tag{13}$$

The matrices written in terms of fundamental nuclei are

$$\begin{aligned}
\mathbf{M}^{ij\tau s} &= I_l^{ij} \triangleright (F_\tau \rho^k \mathbf{I} F_s) \triangleright \\
\mathbf{G}_\Omega^{ij\tau s} &= I_l^{ij} \triangleright (F_\tau \rho^k \mathbf{I} F_s) \triangleright 2\Omega \\
\mathbf{K}^{ij\tau s} &= I_l^{ij} \triangleright \mathbf{D}_{np}^T(F_\tau \mathbf{I})\Big[\tilde{\mathbf{C}}_{np}^k \mathbf{D}_p(F_s\mathbf{I}) + \tilde{\mathbf{C}}_{nn}^k \mathbf{D}_{np}(F_s\mathbf{I})\Big] \\
&\quad + \mathbf{D}_p^T(F_\tau \mathbf{I})\Big[\tilde{\mathbf{C}}_{pp}^k \mathbf{D}_p(F_s\mathbf{I}) + \tilde{\mathbf{C}}_{pn}^k \mathbf{D}_{np}(F_s\mathbf{I})\Big] \triangleright \\
&\quad + I_l^{ij,y} \triangleright \Big[\mathbf{D}_{np}^T(F_\tau\mathbf{I}) + \mathbf{D}_p^T(F_\tau\mathbf{I})\tilde{\mathbf{C}}_{pn}^k\Big] F_s \triangleright \\
&\quad + I_l^{i,yj}\mathbf{I}_{Ay}^T \triangleright F_\tau\Big[\tilde{\mathbf{C}}_{np}^k \mathbf{D}_p(F_s\mathbf{I}) + \tilde{\mathbf{C}}_{nn}^k \mathbf{D}_{np}(F_s\mathbf{I})\Big] \triangleright \\
&\quad + I_l^{i,yj,y}\mathbf{I}_{Ay}^T\mathbf{I}_{Ay} \triangleright F_\tau \tilde{\mathbf{C}}_{nn}^k F_s \triangleright \\
\mathbf{K}_{\sigma_0}^{ij\tau s} &= I_l^{ij} \triangleright (F_{\tau_{,x}}\sigma_{0_{xx}}\mathbf{I}F_{s_{,x}}) + (F_{\tau_{,z}}\sigma_{0_{zz}}\mathbf{I}F_{s_{,z}}) \\
&\quad + (F_{\tau_{,x}}\sigma_{0_{xz}}\mathbf{I}F_{s_{,z}}) + (F_{\tau_{,z}}\sigma_{0_{zx}}\mathbf{I}F_{s_{,x}}) \triangleright \\
\mathbf{K}_\Omega^{ij\tau s} &= I_l^{ij} \triangleright (F_\tau \rho^k \mathbf{I} F_s) \triangleright \Omega^T\Omega \\
\mathbf{F}_\Omega^{i\tau} &= I_l^i \triangleright F_\tau \rho \mathbf{r} \triangleright \Omega^T\Omega
\end{aligned} \tag{14}$$

where

$$\Omega = \begin{bmatrix} 0 & 0 & \Omega \\ 0 & 0 & 0 \\ -\Omega & 0 & 0 \end{bmatrix} \mathbf{I}_{Ay} = \begin{bmatrix} 0 & 0 & 1 \\ 1 & 0 & 0 \\ 0 & 1 & 0 \end{bmatrix} \mathbf{I} = \begin{bmatrix} 1 & 0 & 0 \\ 0 & 1 & 0 \\ 0 & 0 & 1 \end{bmatrix} \tag{15}$$

$$\triangleleft \ \ldots \triangleright = \int_A \ldots dA \tag{16}$$

$$\Big(I_l^i, I_l^{ij}, I_l^{ij,y}, I_l^{i,yj}, I_l^{i,yj,y}\Big) = \int_l (N_i, N_iN_j, N_iN_{j,y}, N_{i,y}N_j, N_{i,y}N_{j,y}) dy \tag{17}$$

Table 1 Frequencies (Hz) at standstill of isotropic cylinders for various α and k

n	TE4	TE5	TE6	TE7	DQM
Supported–supported, $\alpha = 0.02$ and $k = 5$					
1	101.2	101.2	101.2	101.2	101.2
2	96.29	76.25	75.57	64.61	64.61
3	289.4	252.1	189.0	188.1	152.2
Clamped–clamped, $\alpha = 0.02$ and $k = 5$					
1	171.4	171.4	171.4	171.4	170.8
2	115.5	99.35	98.63	90.48	90.17
3	300.7	254.5	192.3	191.2	155.9
Clamped–clamped, $\alpha = 0.005$ and $k = 5$					
2	75.37	73.90	73.84	73.18	72.73
3	178.3	72.94	59.86	59.63	52.50
4	—	215.8	122.6	92.91	75.54
Clamped–clamped, $\alpha = 0.005$ and $k = 3$					
2	168.4	167.5	167.4	167.1	166.6
3	319.1	112.0	104.0	103.6	99.26
4	—	340.9	134.1	107.7	92.38

Note: "n" is the circumferential wave number of the shell.

and $\mathbf{r} = \{x_P, 0, z_P\}$ is the distance of a generic point P belonging to the cross section from the neutral axis. The nine components of the fundamental nucleus of the matrix $\mathbf{K}^{ij\tau s}$ are written in an explicit form in Ref. [32].

The homogeneous equations are solved assuming a periodic solution $\mathbf{q} = \mathbf{q}e^{i\omega t}$ in order to obtain natural frequencies and normal modes of the rotor

$$\mathbf{q}e^{i\omega t}\big[(\mathbf{K} + \mathbf{K}_{\sigma_0} - \mathbf{K}_\Omega) + (\mathbf{G}_\Omega)i\omega - (\mathbf{M})\omega^2\big] = 0 \tag{18}$$

The quadratic eigenvalue problem of Eq. (18) is solved as previously done in Refs. [31] and [32].

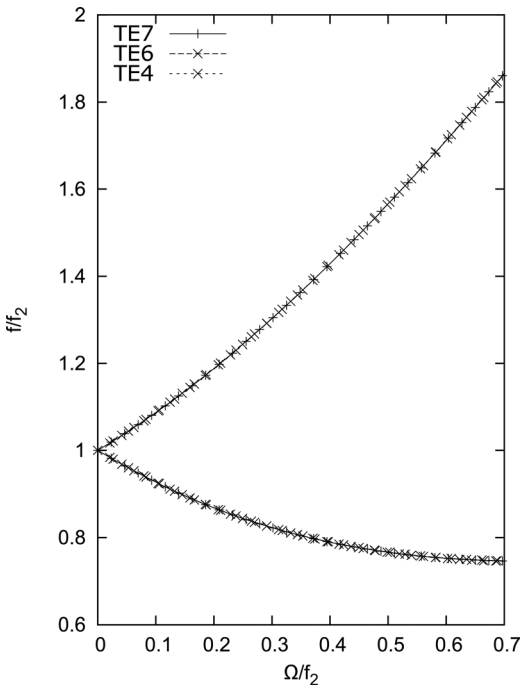

Fig. 2 Dependency of frequency ratio upon the speed parameter for various TE expansions

4 Numerical Results

4.1 Metallic Thin Cylinders. In order to assess the 1D-CUF elements, various analyses have been first performed on thin cylinders in both nonrotating and rotating state. The material is isotropic with Young's modulus ("E"), Poisson's ratio ("ν") and density equal to 207.0 GPa, 0.3 and 7860 kg/m^3, respectively. Table 1 shows the frequencies at standstill for different dimension ratios (α = thickness/diameter and k = length/diameter with diameter equal to 1) obtained with Taylor-like expansions of fourth (TE4), fifth (TE5), sixth (TE6), and seventh (TE7) order. For comparison purposes, the last column shows the frequencies obtained using the Di.Qu.M.A.S.P.A.B. [33] code, free software for plates and shells based on the DQM. As expected, increasing the order of the theory, results converge to reference values for all considered circumferential wave numbers ("n") and boundary conditions. For the supported–supported condition and "n" equal to 2 ($\alpha = 0.02$ and $k = 5$), Fig. 2 shows how the frequency ratio (f/f_n) changes with respect to the speed parameter (Ω/f_n) using the TE4, TE6, and TE7 expansions. In spite of the natural frequencies in the nonrotating state are different, it is interesting to note that the three displacement theories have predicted same variations of backward and forward nondimensional frequencies. In order to evaluate the effects of the boundary condition, cylinders with supported–supported and clamped–clamped ends have been considered. The dimensionless frequencies obtained with the TE7 theory are shown in Figs. 3(*a*) and 3(*b*), respectively. Also in this case, the nondimensional results are nearly identical despite the different frequencies in the nonrotating state (see Table 1). The graphs also show the frequency parameters derived from the following analytical solutions:

$$\frac{f}{f_n} = \frac{2n}{n^2+1}(\Omega/f_n) \pm \sqrt{1 + \frac{n^6 - 2n^4 - 1}{(n^2+1)^2}(\Omega/fn)^2} \tag{19}$$

$$\frac{f}{f_n} = \frac{2n}{n^2+1}(\Omega/f_n) \pm \sqrt{1 + \frac{n^2(n^2-1)^2}{(n^2+1)^2}(\Omega/fn)^2} \tag{20}$$

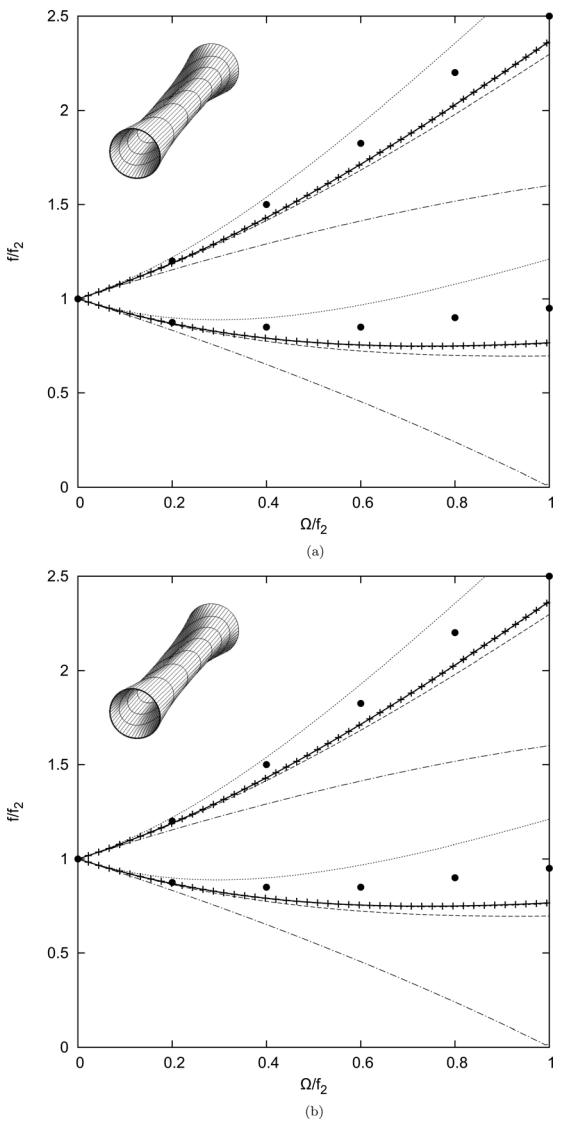

Fig. 3 Dependency of frequency ratio upon the speed parameter. "—": Eq. (19), "– – –": Eq. (20), "- - -": Eq. (21), "•": Ref. [7] of Ref. [11], "· · ·": TE7 w/o σ_0: -·-. (*a*) Supported–supported and (*b*) clamped–clamped.

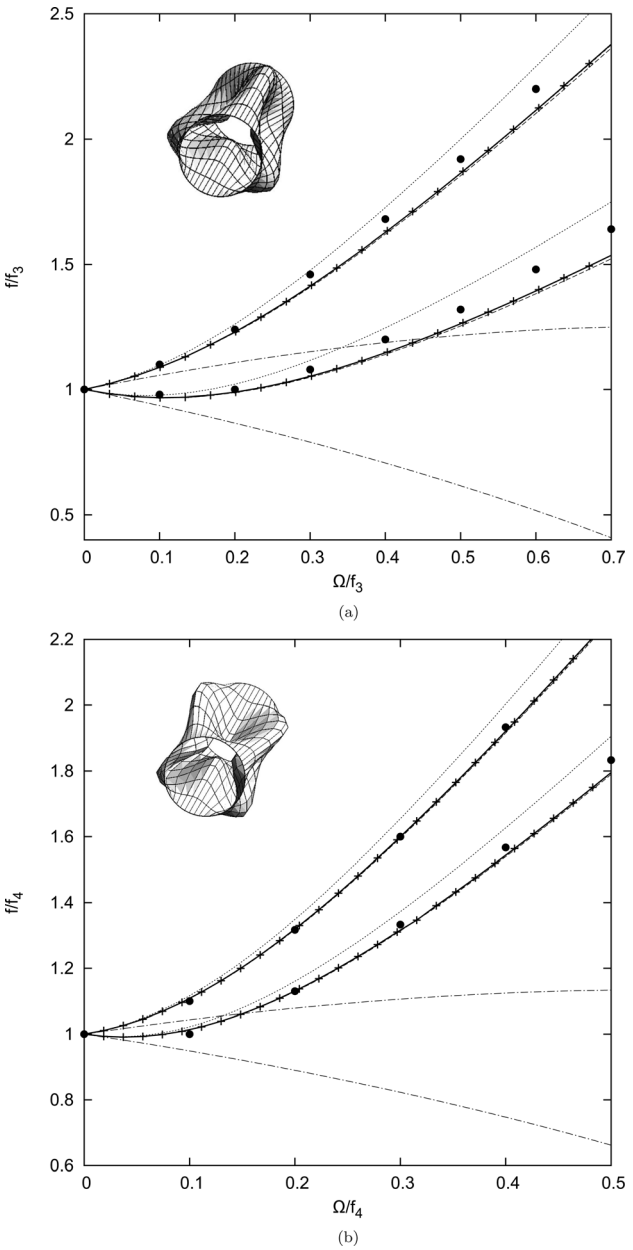

Fig. 4 Dependency of frequency ratio upon the speed parameter. "—": Eq. (19), "– – –": Eq. (20), "- - -": Eq. (21), "•": Ref. [7] of Ref. [11], "· · ·": TE7 w/o σ_0: -·-. (*a*) $k = 5$ and $n = 3$; (*b*) $k = 3$ and $n = 4$.

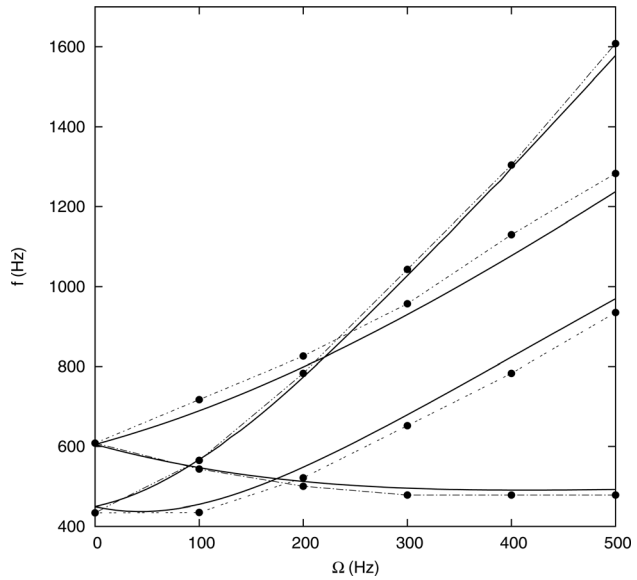

Fig. 5 Dependency of frequency ratio upon the speed parameter. "-•-": Ref. [14] and "—": TE7 ($\alpha = 0.02$ and $k = 0.5$)

$$\frac{f}{f_n} = \frac{2n}{n^2+1}(\Omega/f_n) \pm \sqrt{1 + \frac{n^6+3n^2}{(n^2+1)^2}(\Omega/fn)^2} \tag{21}$$

In particular, Eqs. (19) and (20) were proposed by Endo et al. [11] for the study of rotating rings. Although the solutions were based on a nonlinear shell theory, the expressions present slight differences due to the use of different hypothesis in defining acceleration and strain terms. On the other hand, using the linear approximation, Chen et al. presented in Ref. [13] Eq. (21) for the study of high-speed rotating shells. The other reference values (•) have been taken from Ref. [11], where the results presented in Ref. [9] were reported in the dimensionless form. It should be observed that the TE7 results strongly agree with those obtained using Eq. (20).

Assuming α equal to 0.005, the minimum frequency for the nonrotating cylinder occurs for $n = 3$ (see Table 1). Figure 4(*a*) is the result for this mode. Beam results agree with shell solutions, especially with those of Eqs. (19) and (20). The same consideration can be made for the mode with $n = 4$ ($\alpha = 0.005$ and $k = 3$), whose frequency variations with respect to the rotational speed are shown in Fig. 4(*b*). Table 2 lists dimensionless frequencies for five rotational speeds with or without the geometrical stiffening. It should be observed that the contribution due to the hoop tension becomes more evident as the circumferential wave number increases.

Table 2 Dimensionless frequencies f/f_n versus dimensionless speed Ω/f_n with and without the hoop tension for thin cylinders

		Ω/f_n					
		0.0	0.1	0.2	0.3	0.4	0.5
				Forward			
f/f_2	with σ_0	1.0	0.93	0.87	0.82	0.79	0.77
	w/o σ_0	$1.0^{(0.0)}$	$0.92^{(1.1)}$	$0.83^{(4.6)}$	$0.74^{(9.8)}$	$0.65^{(17.7)}$	$0.55^{(28.6)}$
f/f_3	with σ_0	1.0	0.97	0.99	1.05	1.15	1.26
	w/o σ_0	$1.0^{(0.0)}$	$0.94^{(3.1)}$	$0.87^{(12.1)}$	$0.79^{(24.8)}$	$0.71^{(38.3)}$	$0.62^{(50.8)}$
f/f_4	with σ_0	1.0	1.01	1.13	1.32	1.54	1.79
	w/o σ_0	$1.0^{(0.0)}$	$0.95^{(5.9)}$	$0.89^{(21.2)}$	$0.82^{(37.9)}$	$0.75^{(51.3)}$	$0.66^{(63.1)}$
				Backward			
f/f_2	with σ_0	1.0	1.09	1.19	1.30	1.43	1.57
	w/o σ_0	$1.0^{(0.0)}$	$1.08^{(0.9)}$	$1.15^{(3.4)}$	$1.22^{(6.2)}$	$1.29^{(9.8)}$	$1.35^{(14.0)}$
f/f_3	with σ_0	1.0	1.09	1.23	1.41	1.63	1.86
	w/o σ_0	$1.0^{(0.0)}$	$1.06^{(2.8)}$	$1.11^{(9.8)}$	$1.15^{(18.4)}$	$1.19^{(27.0)}$	$1.22^{(34.4)}$
f/f_4	with σ_0	1.0	1.11	1.32	1.60	1.92	2.26
	w/o σ_0	$1.0^{(0.0)}$	$1.04^{(6.3)}$	$1.08^{(18.2)}$	$1.11^{(30.6)}$	$1.12^{(41.7)}$	$1.13^{(50.0)}$

Note: In brackets, relative errors between the two cases.

Table 3 Frequencies (Hz) at standstill of the thick isotropic cylinder

Modal description			Frequency (Hz)				
Mode type	n	m	TE8	TE9	2D [15]	3D [34]	Exp. [34]
Pure radial	2	0	2746	2606	2573	2594	2570
Radial shearing	2	1	3101	2993	2950	2989	2962
Axial bending	1	1	6233	6230	6239	6240	6286
Global torsion	0	1	6313	6313	6320	6291	—
Radial shearing	2	2	6484	6433	—	6503	6536
Gobal bending	1	2	7038	7033	7134	7109	7104
Radial shearing	3	1	7574	7502	—	7219	7100
Extensional	0	0	8111	8108	8096	8081	8149
Extensional	0	1	8558	8551	—	8567	8615
Extensional	0	2	8821	8815	—	8845	8886
Longitudinal	0	0	11272	11269	11266	11460	11536
Circumferential	1	1	12673	12673	12653	12647	12616

Note: — indicates result not provided.

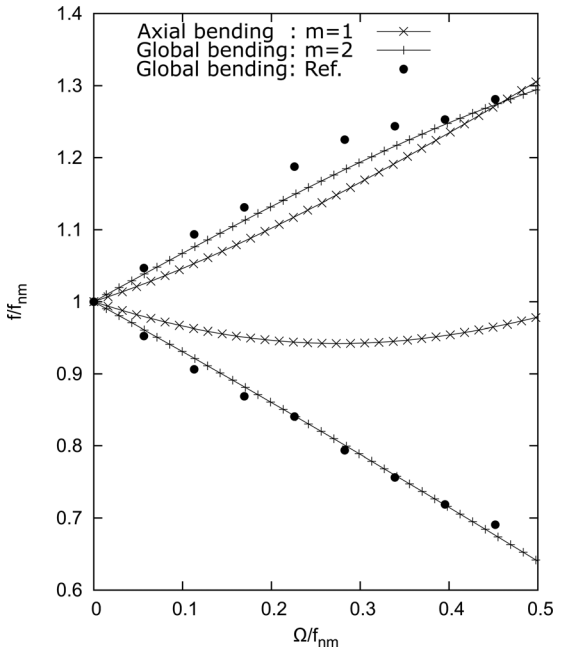

Fig. 6 Dependency of frequency ratio upon the speed parameter of axial bending and global bending modes. TE9, $n = 1$, and Ref. [15].

Other results are presented in Fig. 5, where the frequencies of a rotating cantilevered cylinder ($\alpha = 0.02$ and $k = 0.5$) are shown. In the graph, the branches are related to the modes with $n = 3$ and $n = 2$. The reference solution was taken from Ref. [14], where a finite element based on a nonlinear plant-shell theory was developed. Although there are some slight discrepancies, trends of curves obtained with TE7 expansion are similar to the reference. It is worth noting that the present beam element provides very accurate results for $\Omega = 0$.

4.2 Metallic Thick Cylinder. A thick cylinder with Young's modulus $E = 207$ GPa, Poisson's ratio $\nu = 0.28$, and density $\rho = 7860$ kg/m^3 is here considered. Both ends are free (F–F) and the length, the mean radius and the thickness are 0.254 m, 0.09525 m, and 0.0381 m ($\alpha = 0.2$, $k = 1.333$), respectively. This cylinder was extensively studied in the literature, first at standstill, in order to classify its three-dimensional mode shapes [34] and then, while rotating, with the purpose of evaluating the forward and backward frequencies of these deformation modes [15]. In Table 3, it is possible to observe that Taylor-like expansions (TE8 and TE9) provide results very close to reference frequencies obtained through theoretical and experimental approaches.

The evolutions of a number of frequencies as functions of the rotating speed have been investigated. In these analyses, both radial and circumferential initial stresses have been taken into account.

$$\sigma_{rr} = \rho\Omega^2 \frac{(3-2\nu)}{8(1-\nu)}\left[r_o^2 + r_i^2 - \frac{r_i^2 r_o^2}{r^2} - r^2\right]$$
$$\sigma_{\delta\delta} = \rho\Omega^2 \frac{(3-2\nu)}{8(1-\nu)}\left[r_o^2 + r_i^2 + \frac{r_i^2 r_o^2}{r^2} - \frac{(1+2\nu)}{(3-2\nu)} r^2\right] \tag{22}$$

where "r_i" and "r_o" are the inner and outer radii of the cylinder, respectively. Figure 6 illustrates how frequency parameters change with the rotational speed for global bending ($n = 1$, $m = 2$) and axial bending modes ($n = 1$, $m = 1$). It should be noted that the nonlinear variation of the global bending frequencies predicted by the 1D-CUF elements is quite similar to that presented in Ref. [15]. Figure 7 shows the results for pure radial ($m = 0$) and radial shearing ($m = 1$, 2) modes for n equal to 2 and 3. It is possible to note that a different longitudinal wave number involves changes in the frequency variations, especially for low values of the circumferential wave number n. As also stated in Ref. [15], these differences are not detectable from the above analytical solutions (Eqs. (19) and (21)). Furthermore, Fig. 8 illustrates the variations of the extensional and torsional frequencies. Although nearly constant, the two extensional frequencies exhibit different behavior upon the speed variation. Indeed, the branch related to $m = 0$ grows after $\Omega/f_{00} = 0.25$, while in contrast, for $m = 2$, the frequency decreases after an initial increase. Regarding the torsional frequency, the curve monotonically decreases with the speed, as also shown in Ref. [15].

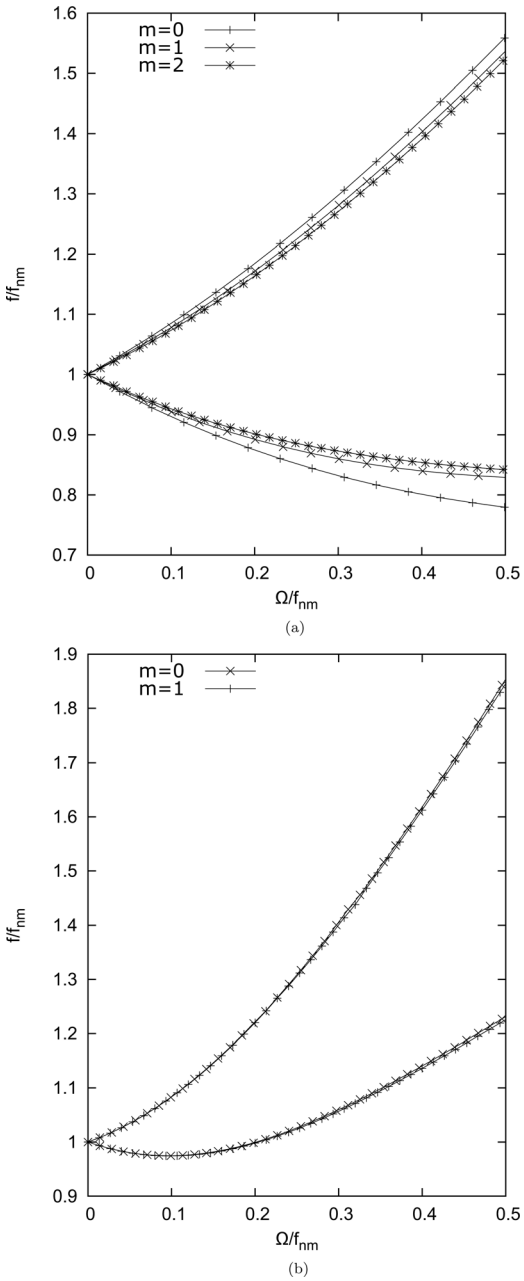

Fig. 7 Dependency of frequency ratio upon the speed parameter of pure radial ($m = 0$) and radial shearing modes ($m = 1$, 2). TE9. (*a*) $n = 2$ and (*b*) $n = 3$.

Similarly to the case of thin cylinders, Table 4 lists forward and backward dimensionless frequencies for various speed parameters, with and without the initial stress. The structure is clamped at both ends, and the frequencies at standstill are $f_2 = 4993.53$ Hz

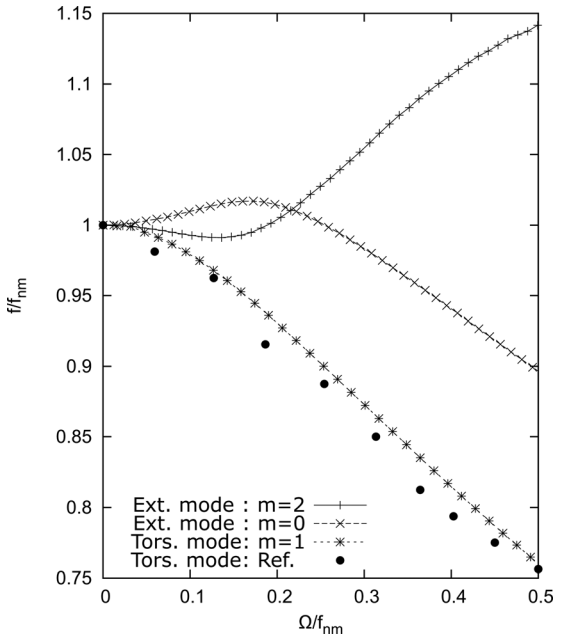

Fig. 8 Dependency of frequency ratio upon the speed parameter of extensional ($n = 0$, 2 and $m = 0$) and global torsion modes ($n = 0$, $m = 0$) TE9, Ref. [15]

and $f_3 = 8435.53$ Hz. Despite the thick wall, natural frequencies are considerably lower when the contribution of the initial stress is overlooked, especially for higher speed values. In addition, relative errors are very close to those computed for the thin cylinder in Table 2.

4.3 Laminated Moderately Thick Cylinders. This section presents the results related to analyses carried out on moderately thick cylinders made of orthotropic material, with the following mechanical properties: $E_{11} = 211$ GPa, $E_{22} = E_{33} = 24.1$ GPa, $G_{12} = G_{13} = G_{23} = 6.9$ GPa, $\nu_{12} = \nu_{13} = \nu_{23} = 0.36$, and $\rho = 1967$ kg/m^3. The thickness-to-diameter and the length-to-diameter ratios are $\alpha = 0.1667$ and $k = 2.5$, respectively, with the mean diameter equal to 0.1 m. The structure is simply supported and clamped at its ends and the layers have the same thickness. The natural frequencies computed with various Taylor-like expansions, and for different lamination schemes, are listed in Table 5. For comparison purposes, in the last column, the results obtained with the DIQUMASPAB software [33] are shown. It should be noted that the beam element TE8 has provided accurate results,

Table 5 Frequencies (Hz) at standstill of the C-S composite cylinder

Mode type	n	M	TE6	TE7	TE8	DQM[a]
			0 deg/0 deg			
Extensional	0	0	10167.	10160.	10160.$^{(0.04)}$	10155.
Bending	1	1	2885.8	2862.4	2862.3$^{(0.16)}$	2857.5
Radial	2	1	3945.9	3827.8	3781.6$^{(3.94)}$	3638.0
Radial	2	2	6498.8	6431.5	6272.5$^{(2.16)}$	6139.7
Radial	3	1	8343.4	8305.3	7978.6$^{(7.07)}$	7451.6
Radial	3	2	9933.8	9855.8	9589.1$^{(6.79)}$	8978.8
Torsion	1	0	3745.9	3745.9	3745.9$^{(0.00)}$	3745.9
			30 deg/−30 deg			
Extensional	0	0	5863.8	5849.7	5849.4$^{(0.26)}$	5833.7
Bending	1	1	5227.5	5206.1	5204.3$^{(-0.42)}$	5226.5
Radial	2	1	4485.7	4308.1	4348.3$^{(2.84)}$	4227.9
Radial	2	2	8315.0	8261.9	8168.3$^{(0.51)}$	8126.1
Radial	3	1	8790.1	8757.7	8459.4$^{(5.93)}$	7985.5
Radial	3	2	10736.	10679.	10429.$^{(5.10)}$	9922.5
Torsion	1	0	8331.1	8322.9	8316.3$^{(-0.82)}$	8385.8
			45 deg/−45 deg			
Extensional	0	0	3637.7	3631.4	3630.3$^{(0.06)}$	3627.9
Bending	1	1	4458.7	4446.6	4444.3$^{(-0.05)}$	4446.9
Radial	2	1	4397.3	4307.9	4271.5$^{(2.71)}$	4158.6
Radial	2	2	7390.9	7311.1	7229.4$^{(0.70)}$	7178.9
Radial	3	1	9649.5	9522.0	9236.3$^{(5.03)}$	8793.7
Radial	3	2	11110.	10989.	10719.$^{(4.98)}$	10210.
Torsion	1	0	9725.8	9710.4	9706.9$^{(-0.66)}$	9771.4
			65 deg/−65 deg			
Extensional	0	0	3288.8	3288.2	3286.8$^{(-0.06)}$	3288.9
Bending	1	1	3496.7	3491.5	3485.6$^{(-0.38)}$	3499.0
Radial	2	1	4886.5	4810.3	4776.1$^{(2.77)}$	4647.0
Radial	2	2	6827.8	6698.8	6624.9$^{(0.83)}$	6570.1
Radial	3	1	11336.	11101.	10679.$^{(5.45)}$	10127.
Radial	3	2	12464.	12189.	11726.$^{(5.76)}$	11087.
Torsion	1	0	8265.4	8242.8	8242.2$^{(-1.55)}$	8372.7
			90 deg/90 deg			
Extensional	0	0	3522.9	3520.9	3520.8$^{(0.54)}$	3501.8
Bending	1	1	2309.3	2302.4	2302.3$^{(0.17)}$	2298.2
Radial	2	1	6344.7	5998.0	5986.4$^{(3.65)}$	5775.2
Radial	2	2	7198.1	6909.6	6851.2$^{(2.46)}$	6686.3
Radial	3	1	14641.	14620.	12836.$^{(6.20)}$	12086.
Radial	3	2	15043.	14918.	13213.$^{(6.17)}$	12444.
Torsion	1	0	3745.9	3745.9	3745.9$^{(0.00)}$	3745.9
			0 deg/90 deg/0 deg			
Extensional	0	0	8735.9	8733.6	8731.0$^{(0.00)}$	8731.7
Bending	1	1	2869.0	2845.3	2845.2$^{(0.20)}$	2839.4
Radial	2	1	4135.6	4044.6	3998.8$^{(4.02)}$	3843.9
Radial	2	2	6597.1	6543.0	6384.8$^{(2.31)}$	6240.5
Radial	3	1	8989.6	8951.6	8621.3$^{(6.83)}$	8069.7
Radial	3	2	10465.	10382.	10104.$^{(6.75)}$	9465.0
Torsion	1	0	3745.9	3745.9	3745.9$^{(0.00)}$	3745.9

[a]First-order shear deformation shell theory.
Note: In brackets, the relative errors: (100*(DQM-TE8))/DQM.

Table 4 Dimensionless frequencies f/f_n versus dimensionless speed Ω/f_n with and without the hoop tension for the thick cylinder

		Ω/f_n					
		0.0	0.1	0.2	0.3	0.4	0.5
				Forward			
f/f_2	with σ_0	1.0	0.93	0.88	0.83	0.80	0.77
	w/o σ_0	1.0$^{(0.0)}$	0.92$^{(1.1)}$	0.84$^{(4.5)}$	0.75$^{(9.6)}$	0.66$^{(17.5)}$	0.56$^{(27.3)}$
f/f_3	with σ_0	1.0	0.97	0.99	1.05	1.12	1.2
	w/o σ_0	1.0$^{(0.0)}$	0.94$^{(3.1)}$	0.87$^{(12.1)}$	0.79$^{(24.8)}$	0.71$^{(36.6)}$	0.62$^{(48.3)}$
				Backward			
f/f_2	with σ_0	1.0	1.09	1.18	1.29	1.45	1.56
	w/o σ_0	1.0$^{(0.0)}$	1.07$^{(1.8)}$	1.14$^{(3.4)}$	1.20$^{(7.5)}$	1.25$^{(13.8)}$	1.30$^{(16.7)}$
f/f_3	with σ_0	1.0	1.08	1.22	1.40	1.62	1.86
	w/o σ_0	1.0$^{(0.0)}$	1.05$^{(2.8)}$	1.09$^{(10.6)}$	1.12$^{(20.0)}$	1.13$^{(30.2)}$	1.14$^{(38.7)}$

Note: In brackets, relative errors between the two cases.

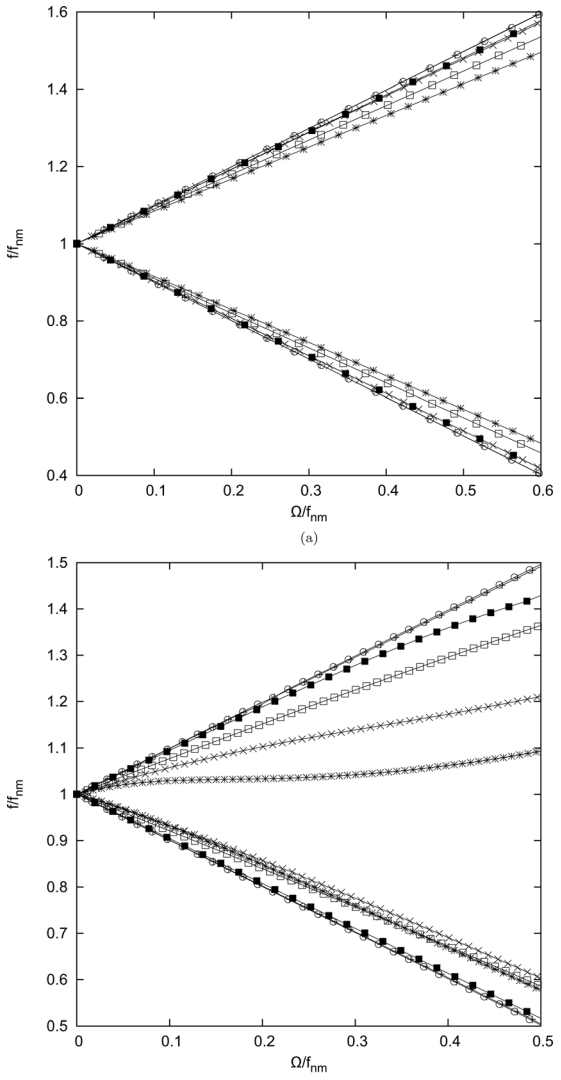

Fig. 9 Dependency of the frequency ratios upon the speed parameter for two different longitudinal wave number. TE8. "-+-": (0 deg/0 deg), "-×-": (30 deg/30 deg), "-*-": (45 deg/45 deg), "-□-": (65 deg/65 deg), "-■-": (90 deg/90 deg), and "-■○■-": (0 deg/90 deg/0 deg). (*a*) $n = 1$ and $m = 1$; (*b*) $n = 1$ and $m = 2$.

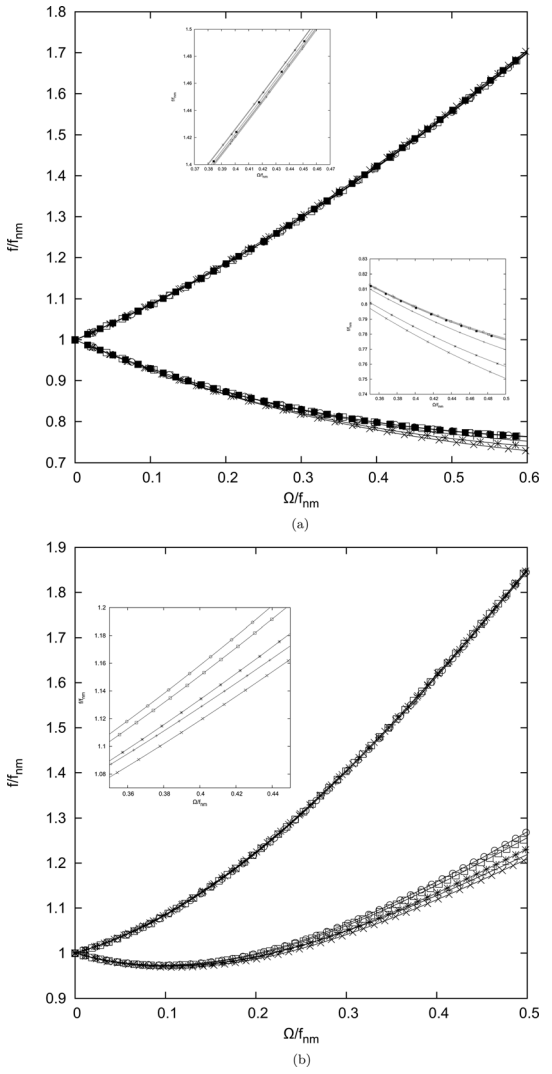

Fig. 10 Dependency of the frequency ratios upon the speed parameter for two different circumferential wave number. TE8. "-+-": (0 deg/0 deg), "-×-": (30 deg/30 deg), "-*-": (45 deg/45 deg), "-□-": (65 deg/65 deg), "-■-": (90 deg/90 deg), and "-■○■-": (0 deg/90 deg/0 deg). (*a*) $n = 2$ and $m = 1$; (*b*) $n = 3$ and $m = 1$.

indeed the maximum percentage error is about 7% for the radial mode with $n = 3$ and lamination scheme (0 deg/0 deg). Furthermore, it should be noted that the lamination scheme strongly affects the order of appearance of modes. For instance, when the ply angle is equal to 90 deg, shell-like modes occur at higher frequencies than those related to bending and extensional deformations, contrary to what happens for 0 deg.

Interesting differences are also observed when the structure is rotating. Figures 9–11 show the frequency parameters as functions of the speed for various lamination schemes. In particular, in the first two graphs, bending frequencies vary almost linearly only when the lamination schemes are (0 deg/0 deg) and (0 deg/90 deg/0 deg). The nonlinear trend of the other curves is much more evident for the angle ply configurations and when the longitudinal wave number, m, is equal to 2 (Fig. 9(*b*)). Figures 10(*a*) and 10(*b*) show the forward and backward branches for n equal to 2 and 3, respectively. Although the influence of the stacking sequence decreases when "n" increases, there remain differences in the frequency variations at higher speed values. Finally, Fig. 11 reveals that the torsional branch variations also depend on the lamination scheme.

5 Conclusion

In this paper, Carrera's Unified Formulation was used to study the dynamics of cylindrical shells. Using Hamilton's principle, the equations of motion were derived and solved with the finite element method. Effects of the initial stress have been included in the present 1D formulation. A number of analyses were carried out considering both thin and thick cylinders with various boundary conditions. The structures were made of either metallic or composite materials. The main results show the following:

- The finite elements based on higher beam models predict frequencies and modal shapes of the cylinders with good accuracy, in both cases of thin and thick walls.
- The 1D-CUF models make it possible to include the initial stress and the related geometrical stiffness matrix.
- The initial stress is essential for the study of both thin and thick cylinders, confirming that classical beam theories are suitable only to study compact cross sections.
- The refined beam models yield reliable results for thick rotating cylindrical shells, contrary to the classical two-dimensional theories, which are most applicable to thin shells.

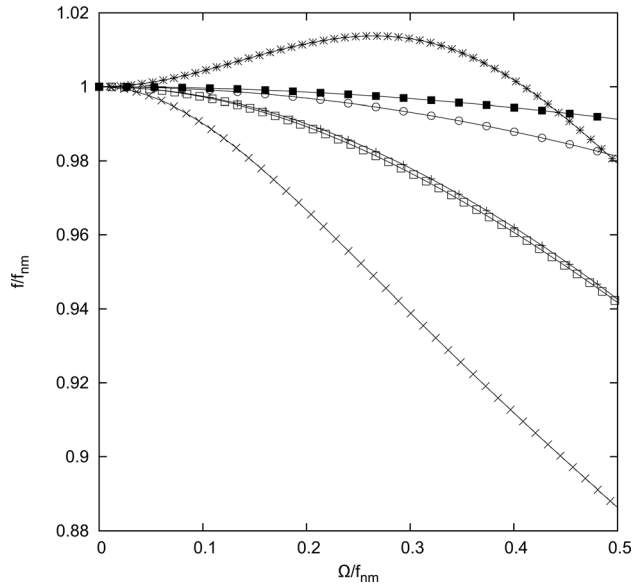

Fig. 11 Dependency of the frequency ratios upon the speed parameter for the torsional mode. TE8, $n = 1$, $m = 0$. "-+-": (0 deg/0 deg), "-×-": (30 deg/30 deg), "-*-": (45 deg/45 deg), "-□-": (65 deg/65 deg), "-■-": (90 deg/90 deg), and "▬○▬": (0 deg/90 deg/0 deg).

- The refined beam elements make it possible to describe the dynamics of laminated cylindrical shells.
- Regarding laminated cylinders, the lamination scheme determines important changes in the trends of the backward and forward frequency branches.

In conclusion, the 1D theory proposed here appears very attractive for the study of rotordynamics, since it ensures accurate results with a low computational effort. Despite being a beam formulation, it allows to include the initial in-plane stresses, both circumferential and radial contributions. In this way, with the same theoretical approach, thick and thin cylinders, deformable disks and arrays of blades can be easily studied. Future work could be devoted, therefore, to the study of more complex spinning structures (conical shells, multisections shaft, etc.) and the effects of longitudinal and transverse stiffeners.

References

[1] Bauer, H. F., 1980, "Vibration of a Rotating Uniform Beam, Part 1: Orientation in the Axis of Rotation," J. Sound Vibration, **72**(2), pp. 177–189.
[2] Curti, G., Raffa, F. A., and Vatta, F., 1991, "The Dynamic Stiffness Matrix Method in the Analysis of Rotating Systems," Tribol. Trans., **34**(1), pp. 81–85.
[3] Curti, G., Raffa, F. A., and Vatta, F., 1992, "An Analytical Approach to the Dynamics of Rotating Shafts," Meccanica, **27**(4), pp. 285–292.
[4] Bauchau, O. A., 1983, "Optimal Design of High Speed Rotating Graphite/Epoxy Shafts," J. Compos. Mater., **17**(3), pp. 170–180.
[5] Chen, L. W., and Peng, W. K., 1998, "The Stability Behavior of Rotating Composite Shafts Under Axial Compressive Loads," Compos. Struct., **41**(3–4), pp. 253–263.
[6] Song, O., and Librescu, L., 1997, "Anisotropy and Structural Coupling on Vibration and Instability of Spinning Thin-Walled Beams," J. Sound Vib., **204**(3), pp. 477–494.
[7] Song, O., Librescu, L., and Jeong, N.-H., 2000, "Vibration and Stability of Pretwisted Spinning Thin-Walled Composite Beams Featuring Bending-Bending Elastic Coupling," J. Sound Vib., **237**(3), pp. 513–533.
[8] Bryan, G. H., 1890, "On the Beats in the Vibration of Revolving Cylinder or Bell," Proc. Cambridge Philos. Soc., **7**(3), pp. 101–111.
[9] Srinivasan, A. V., and Lauterbach, G. F., 1971, "Traveling Waves in Rotating Cylindrical Shells," J. Eng. Ind., **93**(4), pp. 1229–1232.
[10] Padovan, J., 1973, "Natural Frequencies of Rotating Prestressed Cylinders," J. Sound Vib., **31**(4), pp. 469–482.
[11] Endo, M., Katamura, K., Sakata, M., and Taniguchi, O., 1984, "Flexural Vibration of a Thin Rotating Ring," J. Sound Vib., **92**(2), pp. 261–272.
[12] Saito, T., and Endo, M., 1986, "Vibration of Finite Length Rotating Cylindrical Shells," J. Sound Vib., **107**(1), pp. 17–28.
[13] Chen, Y., Zhao, H. B., Shen, Z. P., Grieger, I., and Kröplin, B.-H., 1993, "Vibrations of High Speed Rotating Shells With Calculations for Cylindrical Shells," J. Sound Vib., **160**(1), pp. 137–160.
[14] Guo, D., Zheng, Z., and Chu, F., 2002, "Vibration Analysis of Spinning Cylindrical Shells by Finite Element Method," Int. J. Solids Struct., **39**(3), pp. 725–739.
[15] Guo, D., Chu, F. L., and Zheng, Z. C., 2001, "The Influence of Rotation on Vibration of a Thick Cylindrical Shell," J. Sound Vib., **242**(3), pp. 487–505.
[16] Hua, L., and Lam, K. Y., 1998, "Frequency Characteristics of a Thin Rotating Cylindrical Shell Using the Generalized Differential Quadrature Method," Int. J. Mech. Sci., **40**(5), pp. 443–459.
[17] Sun, S., Chu, S., and Cao, D., 2012, "Vibration Characteristics of Thin Rotating Cylindrical Shells With Various Boundary Conditions," J. Sound Vib., **331**(18), pp. 4170–4186.
[18] Lam, K. Y., and Loy, C. T., 1995, "Free Vibrations of a Rotating Multilayered Cylindrical Shell," Int. J. Solids Struct., **32**(5), pp. 647–663.
[19] Lam, K. Y., and Loy, C. T., 1995, "Analysis of Rotating Laminated Cylindrical Shells by Different Thin Shell Theories," J. Sound Vib., **186**(1), pp. 23–35.
[20] Lam, K. Y., and Loy, C. T., 1998, "Influence of Boundary Conditions for a Thin Laminated Rotating Cylindrical Shell," Compos. Struct., **41**(3–4), pp. 215–228.
[21] Civalek, Ö., 2007, "A Parametric Study of the Free Vibration Analysis of Rotating Laminated Cylindrical Shells Using the Method of Discrete Singular Convolution," Thin-Walled Struct., **45**(7), pp. 692–698.
[22] Ramezani, S., and Ahmadian, M. T., 2009, "Free Vibration Analysis of Rotating Laminated Cylindrical Shells Under Different Boundary Conditions Using a Combination of the Layerwise Theory and Wave Propagation Approach," Scientia Iranica Trans. B: Mech. Eng., **16**(2), pp. 168–176.
[23] Liu, L., Cao, D., and Sun, S., 2013, "Vibration Analysis for Rotating Ring-Stiffened Cylindrical Shells With Arbitrary Boundary Conditions," ASME J. Vib. Acoust., **135**(6), p. 061010.
[24] Lee, Y. S., and Kim, Y. W., 1998, "Vibration Analysis of Rotating Composite Cylindrical Shells With Orthogonal Stiffeners," Comput. Struct., **69**(2), pp. 271–281.
[25] Zhao, X., Liew, K. M., and Ng, T. Y., 2002, "Vibrations of Rotating Cross-Ply Laminated Circular Cylindrical Shells With Stringer and Ring Stiffeners," Int. J. Solids Struct., **39**(2), pp. 529–545.
[26] Hua, L., Khin-Yong, L., and Ng, T.-Y., 2005, *Rotating Shell Dynamics* (Studies in Applied Mechanics), Elsevier, Oxford, UK.
[27] Carrera, E., Giunta, G., and Petrolo, M., 2011, *Beam Structures: Classical and Advanced Theories*, Wiley, West Sussex, UK.
[28] Carrera, E., Zappino, E., and Filippi, M., 2013, "Free Vibration Analysis of Thin-Walled Cylinders Reinforced With Longitudinal and Transversal Stiffeners," ASME J. Vib. Acoust., **135**(1), p. 011019.
[29] Carrera, E., Filippi, M., and Zappino, E., 2013, "Laminated Beam Analysis by Polynomial, Trigonometric, Exponential and Zig-Zag Theories," Eur. J. Mech. A/Solids, **41**, pp. 58–69.
[30] Carrera, E., Filippi, M., and Zappino, E., 2014, "Free Vibration Analysis of Laminated Beam by Polynomial, Trigonometric, Exponential and Zig-Zag Theories," J. Compos. Mater., **48**(19), pp. 2299–2316.
[31] Carrera, E., Filippi, M., and Zappino, E., 2013, "Analysis of Rotor Dynamic by One-Dimensional Variable Kinematic Theories," ASME J. Eng. Gas Turbines Power, **135**(9), p. 092501.
[32] Carrera, E., and Filippi, M., 2014, "Variable Kinematic One-Dimensional Finite Elements for the Analysis of Rotors Made of Composite Materials," ASME J. Gas Turbines Power, **136**(9), p. 092501.
[33] Viola, E., Tornabene, F., and N. Fantuzzi, N., "DiQuMASPAB (Differential Quadrature for Mechanics of Anisotropic Shells, Plates, Arches and Beams)," DICAM Department, Alma Mater Studiorum, University of Bologna, Bologna, Italy, http://software.dicam.unibo.it/diqumaspab-project
[34] Wang, H., Williams, K., and Guan, W., 1998, "A Vibrational Mode Analysis of Free Finite-Length Thick Cylinders Using the Finite Element Method," ASME J. Vib. Acoust., **120**(2), pp. 371–377.